Is the tidal triggering of earthquakes at Axial Seamount predictive of eruptions?

Anders Carlson

University of Washington

School of Oceanography, Box 357940

Seattle, WA 98195-7940

anders03@uw.edu

Abstract

Scientists have long hypothesized that tidal forces can trigger earthquakes due to the change in stress along a fault. This phenomenon is called tidal triggering of earthquakes. My study investigated the tidal triggering of earthquakes at Axial Seamount, Juan de Fuca Ridge from the time of the last eruption in 2015, to the present. This study tests the validity of the correlation between tidal triggering and volcanic cycles. My hypothesis is that the fraction of earthquakes is highest at low tidal heights / phases, and that tidal triggering increases in strength over time, therefore a potential sign during the onset of an eruption. Using data from the Ocean Observatories Initiative Regional Cabled Array, and the Oregon State University Tidal Model, I interpolated the time of earthquakes with the tidal cycle. Data from an earthquake catalog was plotted against the tidal model. Results prove my hypothesis to be valid. On an annual basis, the highest percentage of earthquakes occur within 30° of lowest tide (180°), and the highest rate of earthquakes per hour occur between -2m to -1m tidal height. On average, the percentage of earthquakes between 150° to 210° increases annually with a slope 1.88 %/y. Additionally, the relative rate of earthquakes at -2m to -1m increases by 0.24 per year. I propose that the Axial Seamount will erupt soon, given tidal triggering has increased in strength and current data reflects similar data to what was seen prior to the 2015 eruption.

Plain Language Summary

As the gravitational pull from the sun and moon causes the ocean tides to rise and fall, there is a change in stress exerted on Axial Seamount. Axial Seamount is located on the Juan de Fuca Ridge approximately 500km west of Pacific City, Oregon. Stress induced is dictated by pressure from the volume of water on the ocean crust complemented by gravity. When the tide

height lowers, there is less water volume pushing down on the sea floor. As tide height varies during the tidal cycle, there is a change in stress from high to low, which causes the fault line at Axial Seamount to slip. High stress correlates to high tide height, and low stress correlates to low tidal height. Stress pushing down on the fault is removed at low tide, and creates slipping of the fault. Through correlating tidal cycle data and earthquake data, this research study tested to see if the earthquakes occurring at Axial Seamount were preferable at low tide. Additionally, I investigated if the strength of this phenomenon increased proportionally with time from 2015 to 2021. Through comparing data prior to the last eruption in 2015, I investigated if we are seeing similar trends in seismic activity to the last eruption, in order to predict the next eruption. My study found that earthquakes are occurring preferably at low tide, and that Axial Seamount is showing similar seismic activity of what was seen prior to the last eruption. This study is important in the context of volcanism on a local and global scale. Volcanoes are present in many regions of the ocean and on continents. By understanding the relation to tidal triggering of earthquakes, we can better understand the seismic activity and eruption potential. Eruption information is important for knowing to stay clear of these events.

Introduction

The phenomenon of tidal triggering of earthquakes was established more than twelve decades ago. It is credited to gravitational forces and the effect they have on the height of Earth's continental surface and ocean (Schuster, 1987, Heaton, 1975). Tidal triggering of earthquakes occurs when there is a change in stress on fault lines due to the gravitational pull on the surface of either the continental crust or ocean. The height deviation from the mean surface level of the continental crust or the ocean water level changes the amount of stress induced on

the respective fault line. Gravitational forces from the pull of the sun and moon can change the surface height of the crust up to 40cm, while in the ocean, there are shifts in sea level height up to meters in magnitude (Heaton, 1975). This change in stress on the fault causes earthquakes.

One of the earliest papers to give an in-depth report of tidal triggering came from Berg (1966), where after a 1964 Alaskan earthquake, most of its aftershocks occurred at low tide. However, during the early study of this phenomenon, there were findings which both supported and disagreed with the correlation between tidal triggering and earthquakes. Contrary to the paper from Berg (1966), the study by Vidale et al. (1998) provided a solid overview on the relation between tidal stresses on fault planes and earthquake activity. This research was conducted by looking at stress accumulation and tidal triggering of earthquakes close to the San Andreas and Calaveras faults. Vidale et al. (1998) did not find any clear effect of the tidal stress change on when the earthquake rupture started.

Following the study of Vidale et al. (1998), another study conducted by Tolstoy et al. (2002) investigated activity at the Axial Seamount. In this paper, findings indicate that earthquakes relative to the ocean tides are occurring preferentially at, or near low tide. This was identified by the harmonic tremor observed on all instruments, correlating with low tides. These findings are also consistent with Wilcock (2001), which made the conclusion that earthquakes occur more frequently near low tides at the Endeavour Segment of the Juan de Fuca Ridge. This finding was reported with a high level of confidence.

While both the continental region and the ocean basin are affected by tidal stress, ocean faults experience a higher magnitude of stress in comparison to land tides (Tolstoy et al., 2002). This difference is because of the greater amplitude of ocean tides, therefore causing a larger stress on the fault when the water shifts between high and low tide (Wilcock, 2001). Therefore,

this explains the differing findings by Vidale et al. (1998), since this study near the San Andreas and Calaveras faults was conducted on land. Since tidal triggering is more defined in the ocean, I chose to research tidal triggering in the ocean basin. I conducted my research at the Axial Seamount.

The Juan de Fuca Ridge is an important area of volcanism as it is one of 18 locations on Earth where hot spots and mid-ocean ridge systems interact (Chadwick et al., 2005). The Axial Seamount is the most prominent bathymetric feature on the Juan de Fuca ridge, rising up from the seafloor to 1500m below sea level (Chadwick et al., 2005). Axial Seamount can be studied in depth because of the presence of the sophisticated regional cabled array. The regional cabled array provides quick, real-time data from the Juan de Fuca Ridge and Axial Seamount. Data is transferred to laboratories through an expanse of fiber-optic cables stretched ~500km off the Oregon Coast (Kelley et al., 2014). The cabled array was installed in 2014 and has been of importance ever since for those researching the Juan de Fuca Ridge (Fig. 1).

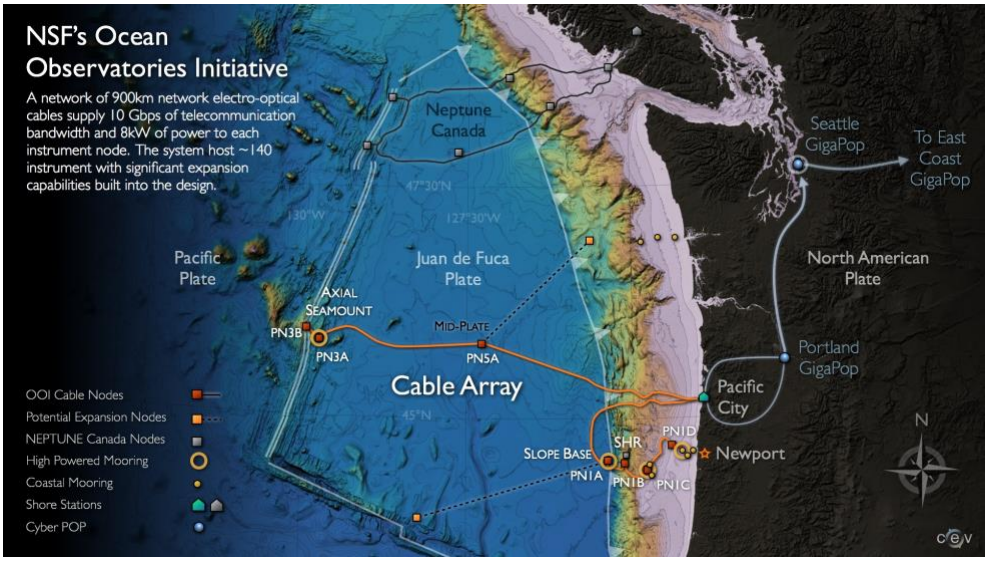

Figure 1. *Map of the Juan de Fuca Ridge and span of the Cabled Array. (Reproduced from Kelley et al., 2014)*

The most recent eruption of the Axial Seamount in 2015 has led to the continued study of this region. At the top of the seamount is a caldera, which is the focus of this study (Fig. 2).

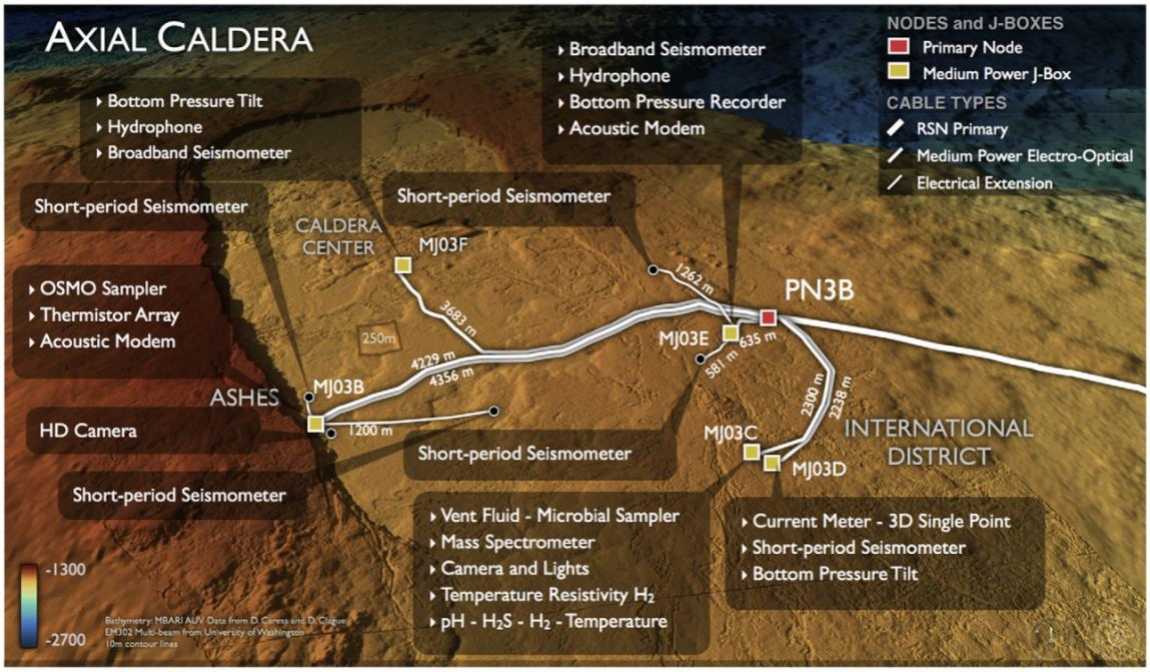

Figure 2. *The Axial Caldera and instruments present. The presence of short-period and broadband seismometers are the most important instruments in registering earthquakes to send back through the cabled array (Reproduced from Kelley et al., 2014).*

The caldera is a horseshoe-shaped 3km x 8km feature, which trends 170°, deepest on the northwest side, with the southeast rim buried by lava flows. The magma chamber of the caldera inflates and deflates relative to the tidal pressure, which is present on top of the caldera ring fault (Fig. 3).

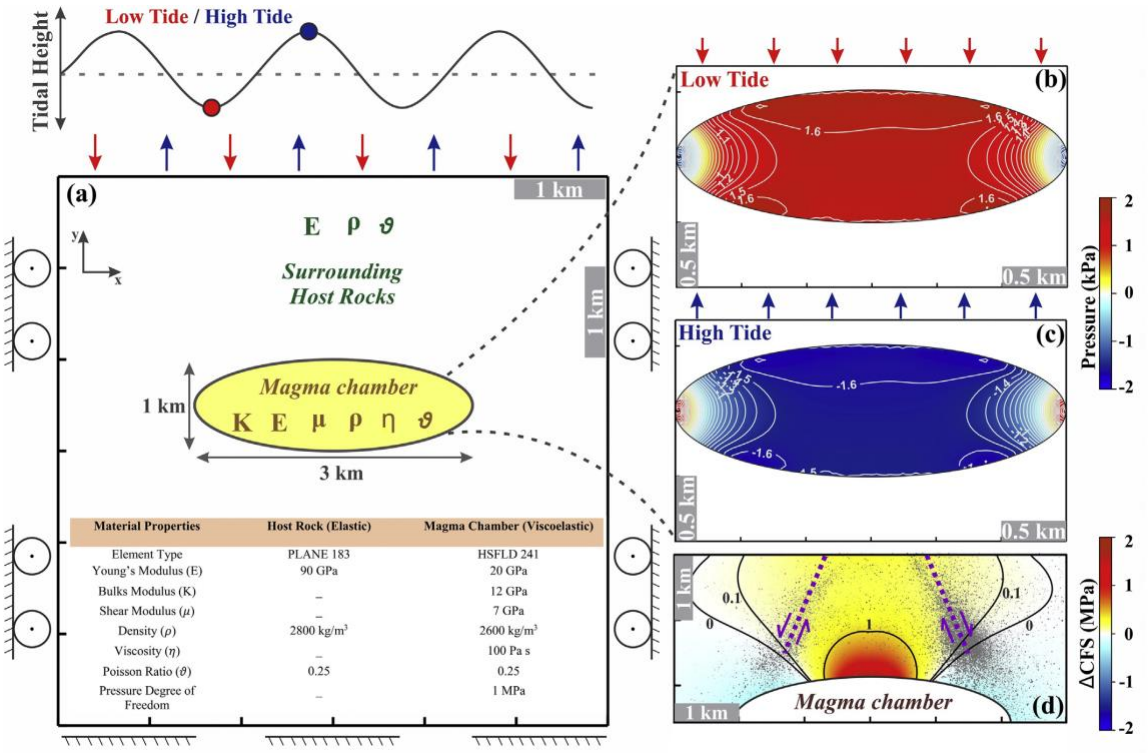

Figure 3. *Tidal phases and magma chamber correlation. The top left of this figure displays the color coordination of high and low tides relating to pressure of the magma chamber in (b) and (c). Positive pressure indicates inflation while negative pressure indicates deflation. (d) Displays a vertical profile of pressures on the magma chamber. (Reproduced from Sahoo et al., 2021)*

In this figure a positive pressure denotes that there is inflation in the magma chamber due to the relieved stress. This is due to reduced water pressure on top of the chamber at low tide. Because of reduced stress, this would cause the caldera ring fault to slip and trigger earthquakes on a periodic basis. Fig. 4 from Wilcock et al. (2018), displays how the caldera inflation causes earthquakes and eventually leads to the rupture and eruption of the seamount.

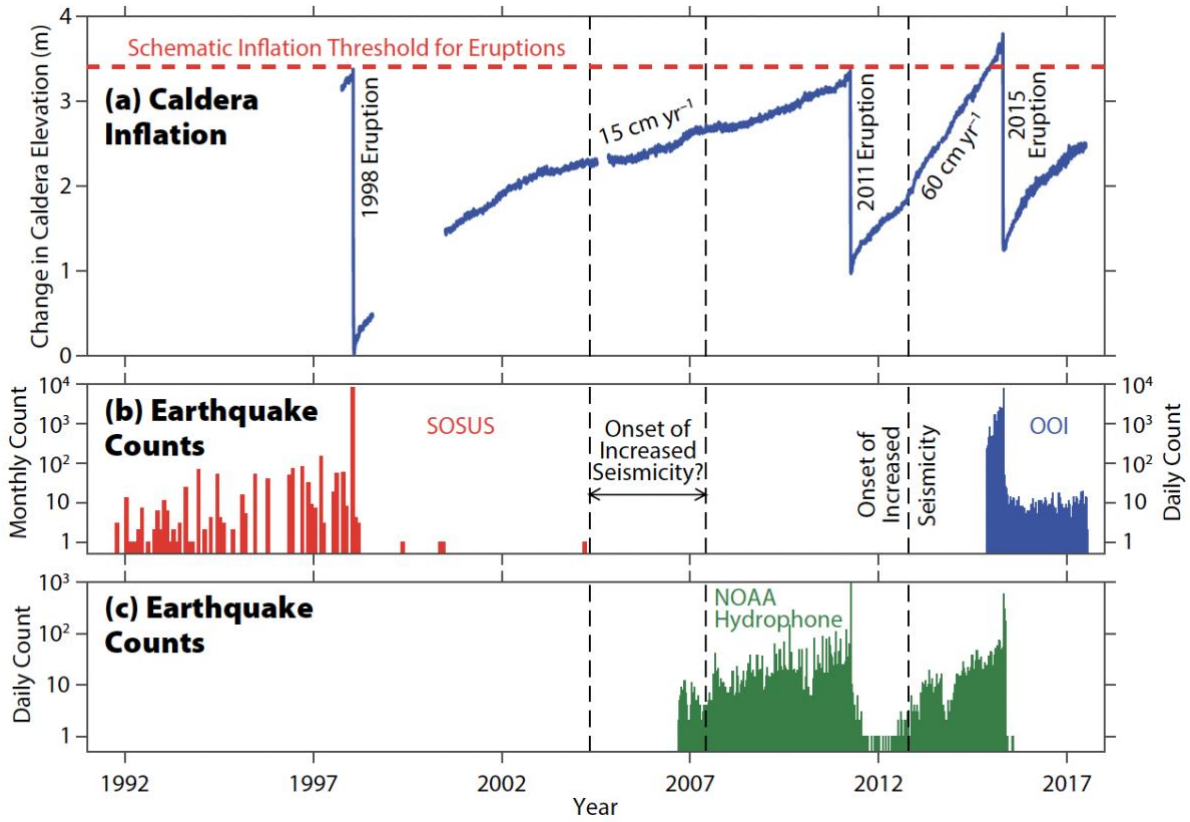

Figure 4. *(a) Caldera inflation recorded in centimeters per year dating back to the 1998 eruption. Gradual increase in inflation is present until each corresponding eruption occurs, and caldera elevation reverts back to pre-eruption levels to increase again. (b) Earthquake counts on a monthly basis from the combination of data from The Sound Surveillance System from the US Navy (SOSUS) and Ocean Observatories Initiative (OOI). (c) Earthquake daily counts dating 2006 to 2015 from the NOAA Hydrophone (Reproduced from Wilcock et al., 2018).*

Since the installation of the cabled array and tracking the 2015 eruption of the Axial Seamount, there have been more studies which increase the confidence in the correlation between tidal triggering and earthquake activity. With the new tools to track this activity, just prior to the eruption, there was a heightened quantity of seismic activity showing inflation of the caldera is correlated with strong tidal triggering, thus indicating a critically stressed system (Wilcock et al., 2016). This heightened activity is shown in Fig. 5 from Wilcock et al. (2016), and correlates with Fig. 4(a), depicting caldera inflation at its highest in 2015.

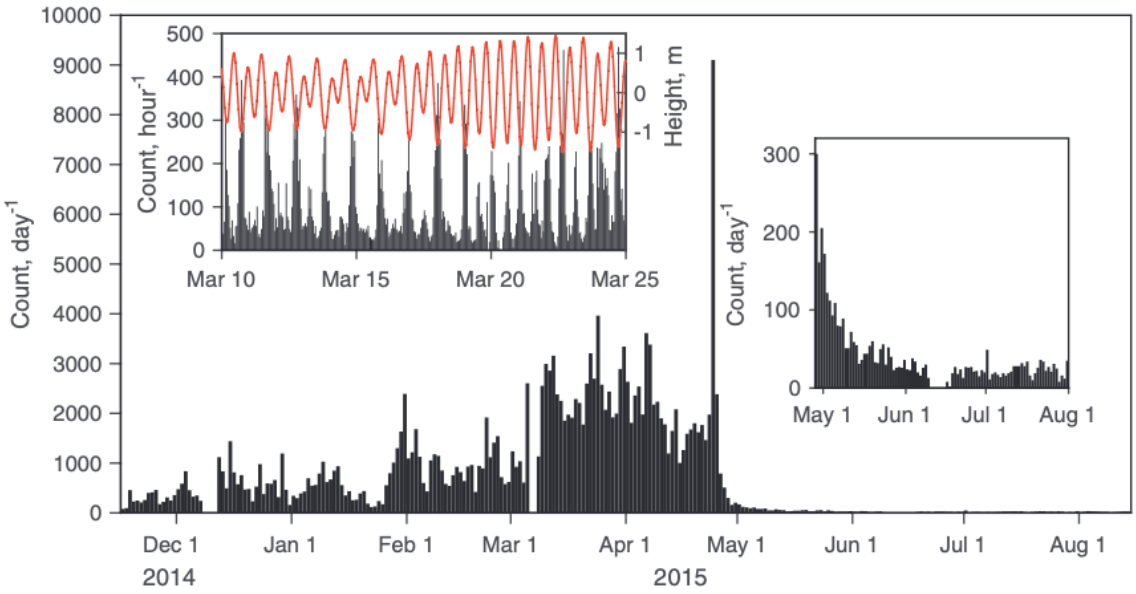

Figure 5. *Histogram of earthquake count per day 9 months spanning the 2015 eruption. (Right insert) Earthquake count per day following the eruption. (Left insert) Earthquake rate per hour between March 10 – 15, 2015, superimposed with tidal height during that time.*
(Reproduced from Wilcock et al., 2016)

Following this paper, Scholz et al. (2019), was able produce more evidence that the magma chamber inflated and deflated in response to tidal stress, therefore leading to the shallow earthquake depths. This research adds more support to confidence in tidal triggering.

Through my study, I aimed at continuing research in this field by investigating data following the 2015 eruption at the Axial Seamount. The reason for my research is to test the relationship between the tidal cycle and seismic activity on an annual basis. The specific event I studied has to do with the slip of a fault from the change in stress of the semi-diurnal tide due to gravitational pull (Heaton, 1975). I looked for evidence of tidal triggering among total earthquake counts and what it meant for eruption predictions. My hypothesis is that there is a higher fraction of earthquakes that occur preferential at low tide, and that tidal triggering increases in strength approaching an eruption. If the correlation is true, earthquake percentage is highest during the low tidal phases, and rate of earthquakes per hour increases, the lower the tidal

height. Tidal triggering strength increasing would be reflected by an annual increase in percentage of earthquakes at a low tidal phase, and higher relative rate of earthquakes at a low tidal height. Further, if I am able to prove my hypothesis I will compare data leading up to the 2015 eruption to the present, and make a prediction of when the next eruption will take place.

Methods

This research study used data from the Axial Seamount Earthquake Catalog recorded from the Ocean Observatories Initiative (OOI) cabled observatory (Wilcock et al., 2016, 2017). Shown in Table 1, reproduced from Kelley et al. (2014), is the list of instruments at the Axial Seamount and Endeavour Segment. The instruments that were most important in this research include the broadband seismometer with accelerometer, and the short period seismometers. The seismometer provided information on earthquakes which was correlated with Oregon State University's (OSU) Tidal Model. This correlation determined tidal stress changes and therefore investigation into tidal triggering at the Axial Seamount.

Table 1

Instrumentation present at Axial Seamount and Endeavour Segment, which provide real-time data to OOI and Neptune Canada, respectively (Reproduced from Kelley et al., 2014).

Instrumentation at Axial and Endeavour.

	Axial[a]	Endeavour[b]	Measurements
Broadband seismometer with accelerometer	X	X	Global large magnitude earthquakes, melt migration, tremor
Short-period seismometers	X	X	Local earthquakes, melt and fluid migration, whale calls
Low frequency hydrophone	X		Acoustic tertiary waves of earthquakes
Bottom pressure sensor	X	X	Tides, storms, tsunamis
Current meter	X	X	Local currents
Bottom pressure – tilt instrument	X		Deflation and inflation of seafloor
Remote access fluid sampler	X	X	Chemistry of diffuse flow
Osmo fluid sampler	X		Chemistry of diffuse flow
DNA sampler	X		Microbial DNA, community structure
Temperature–resistivity–H_2	X	X	Black smoker fluid temperature, chlorinity, and hydrogen to monitor boiling, fluid–rock reactions
Temperature–pH–H_2S–H_2	X		Black smoker fluid temperature, acidity, hydrogen sulfide, and hydrogen concentrations to monitor boiling and changes in the reaction zone
Temperature–thermistor array	X	X	3D and linear temperature distribution in diffuse flow site
Mass spectrometer	X		Dissolved gas concentrations (e.g. carbon dioxide, methane, hydrogen sulfide) in diffuse flow
Digital still camera	X		Diffuse flow and black smoker sites – macrofauna and microbial distribution, changes in flow, smoker growth
High definition camera	X	X	Diffuse flow and black smoker sites – macrofauna and microbial distribution and changes in flow, smoker growth
Acoustic Doppler current profiler	X	X	Larger scale current velocities than current meter
Plume imager (COVIS)		X	Hydrothermal plume fluctuations combined with temperature measurements provide heat flux calculations
CTD	X	X	Conductivity, temperature, depth, ±dissolved oxygen of seawater and plumes

Seismicity data from the earthquake catalog is transferred back to the OOI through the expansive regional cabled array. The earthquake catalog is updated hourly, therefore producing

real-time data. During certain periods of high sample rate, earthquake data is disrupted by the Navy for security reasons. However, the data is later backfilled to create a mostly full and accurate catalog within the bounds of Navy's security. The earthquake catalog provides a series of variables, such as earthquake occurrence, earthquake depth, and earthquake location at the caldera. Fig. 6 (a) and (b), reproduced from Wilcock et al. 2016, 2017, are examples of both when earthquakes registered, and a plot of location and depth of earthquakes.

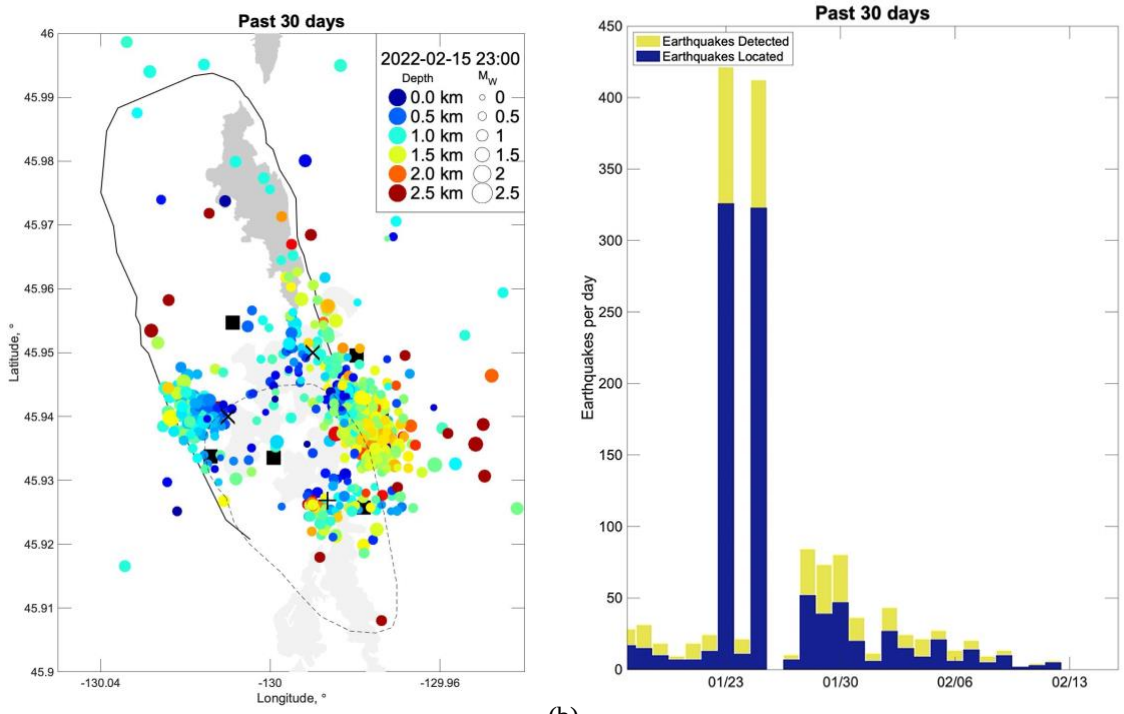

(a) (b)

Figure 6. *(a) Location and depth of earthquakes in past 30 days. (b)Earthquakes per day in the last 30 days at Axial Seamount. (Reproduced from Wilcock et al., 2016, 2017)*

For this study I used the times of these earthquakes were registered. I compared this seismic data from the earthquake catalog with the OSU Tidal Model data at the Axial Seamount (Egbert et al., 2002). The OSU Tidal model produces global, regional, and local models with OSU Tidal Inversion Software by assimilating satellite altimetry. By considering bathymetry /

depth grid (m), elevations, and transports (m^2/s), tidal elevations and tidal phases are computed and made available for analysis (Egbert et al., 2002).

Tidal phase is measured on a scale of 0° - 360° with 0° and 360° representing high tide and 180° for low tide. Tidal stress is measured on a scale of force per area. In this case the normal and shear stress is analogous to tidal height. A higher stress means higher tide height and vice versa. Shown in Fig. 7, reproduced from Heaton (1975), is an example of the typical relation between tidal stress and tidal phase.

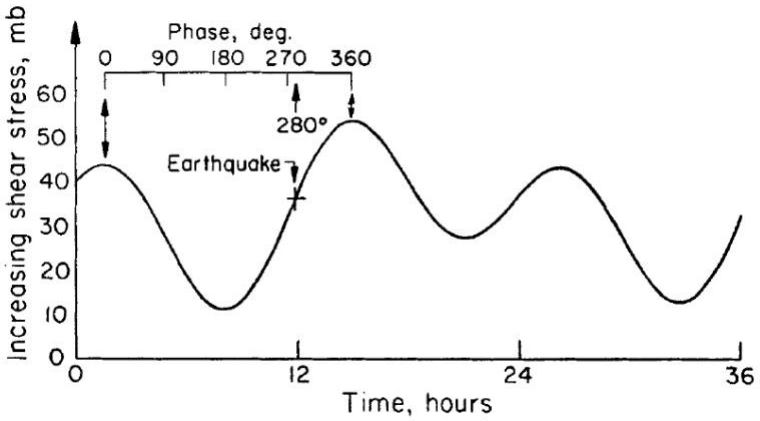

Figure 7. *Tidal phase and time vs. stress, denoting activity (Reproduced from Heaton, 1975).*

A higher tide height means a greater volume of seawater pushing down on seafloor, and in the context of this study, the caldera of the Axial Seamount. This figure represents a semi-diurnal tidal cycle where there are two high and two low tides every 24 hours. At Axial Seamount, the tides are semi-diurnal where there are two high and two low tides with amplitudes that differ, each day.

I used MATLAB to correlate the data series of earthquake occurrence, tidal height, and tidal phase to plot annual histograms. I interpolated the tidal phases to the earthquake times. Plots showed the fraction of earthquakes occurring at certain tidal phases in comparison to all

other tidal phases for the year. In plotting the histograms this way, it allowed me to see the dominant tidal phase earthquakes were occurring at.

Plotting tidal height varies compared to tidal phase because of the need to account for the proportion of tidal heights at extremely low tide heights. Extreme low tide heights occur rarely, so I accounted for this to represent an accurate earthquake rate as tidal data is reported every 5 minutes. The data was plotted in a range of bins from – 2 m (low tide) to 2 m (high tide). On an annual basis, earthquake occurrence is represented as a rate of earthquakes per hour.

I used this data to create scatter plots to compare data on an annual basis and look for trends. For tidal phase, this was completed by summing the fraction of earthquakes in the two bins occurring between 150° and 210°, which represent low tide. For tidal height, I calculated the relative rate of earthquakes at low tide by measuring the rate at heights of -2m to -1m and dividing it by the average rate during the year.

Results

There is a correlation between tidal phase and earthquake percentage for the semi-diurnal tide cycle occurring at the Axial Seamount (Fig. 8). The phase between 150° and 210° correlates to when low tide is occurring based on tidal height registered in the tidal model. Furthermore, this is displayed by the highest percentage of earthquakes in this phase range. Most times annually, the two bins between 150°- 210° register the highest percentage of earthquakes compared to all earthquakes during that year. There are peaks of highest percentage that stray from the 150°- 210° range during 2015, 2019, and 2021.

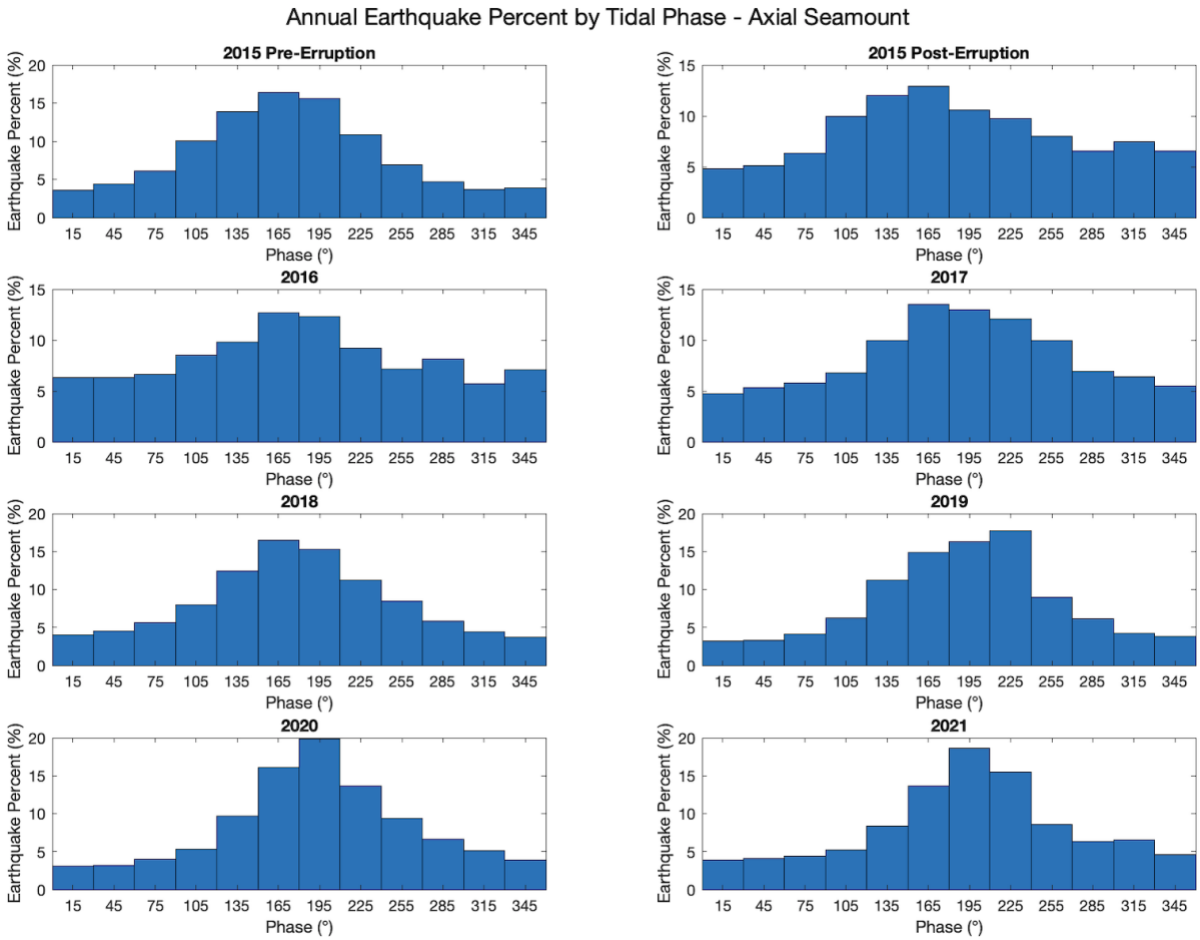

Figure 8. *Panel of annual histograms from June 1, 2015, to December 2, 2021 for post eruption data. January 22, 2015 to April 22, 2015 plots data for 2015 just prior to the eruption, which occurred in 2015. Each histogram plots the percent of earthquakes occurring at a specific tidal phase annually. Plots are normalized to represent a percentage of earthquakes per phase in comparison to the total earthquakes that occurred (out of 100%). The tidal phase ranges from 0° to 360° with bin width being 30°.*

On an annual basis there is a direct correlation represented by a linear fit line on the scatter plot between earthquake percentage and time (Fig. 9). With a positive slope increasing with time from 2015 post-eruption to 2021, it is evident that the fraction of earthquakes is increasing at the low tidal phase following the eruption. Each year, there is a higher fraction of total earthquakes that are occurring during the low tidal phase of 150° – 210°. The slope of this trend is 1.9%/y and has an R^2 value of 0.88.

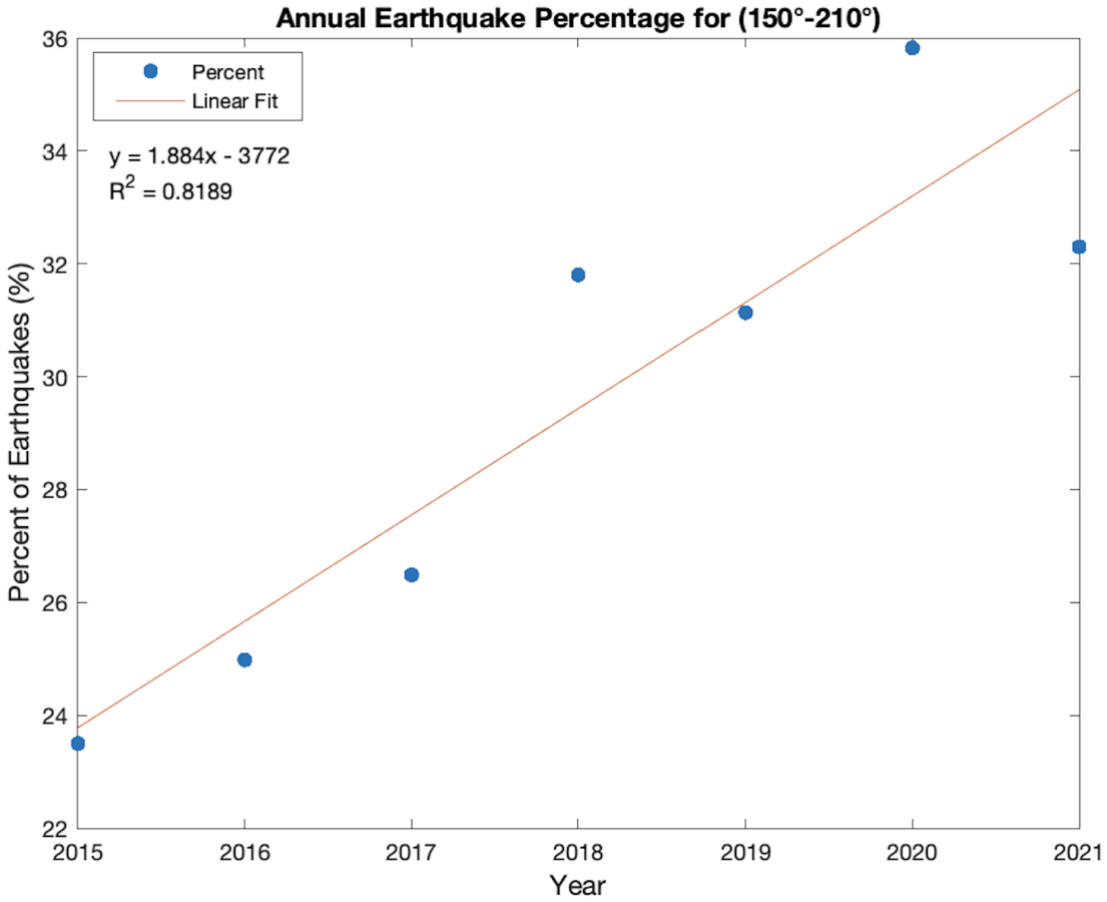

Figure 9. *Scatter plot of annual data for earthquake percentage which summed the fraction of earthquakes between 150°-210° and plotted for each year.*

Earthquake rate is most dominant at the lowest tidal heights represented annually for earthquakes per hour (Fig. 10). The rates of earthquakes drop substantially after the -1m tidal height bin as tide height increases.

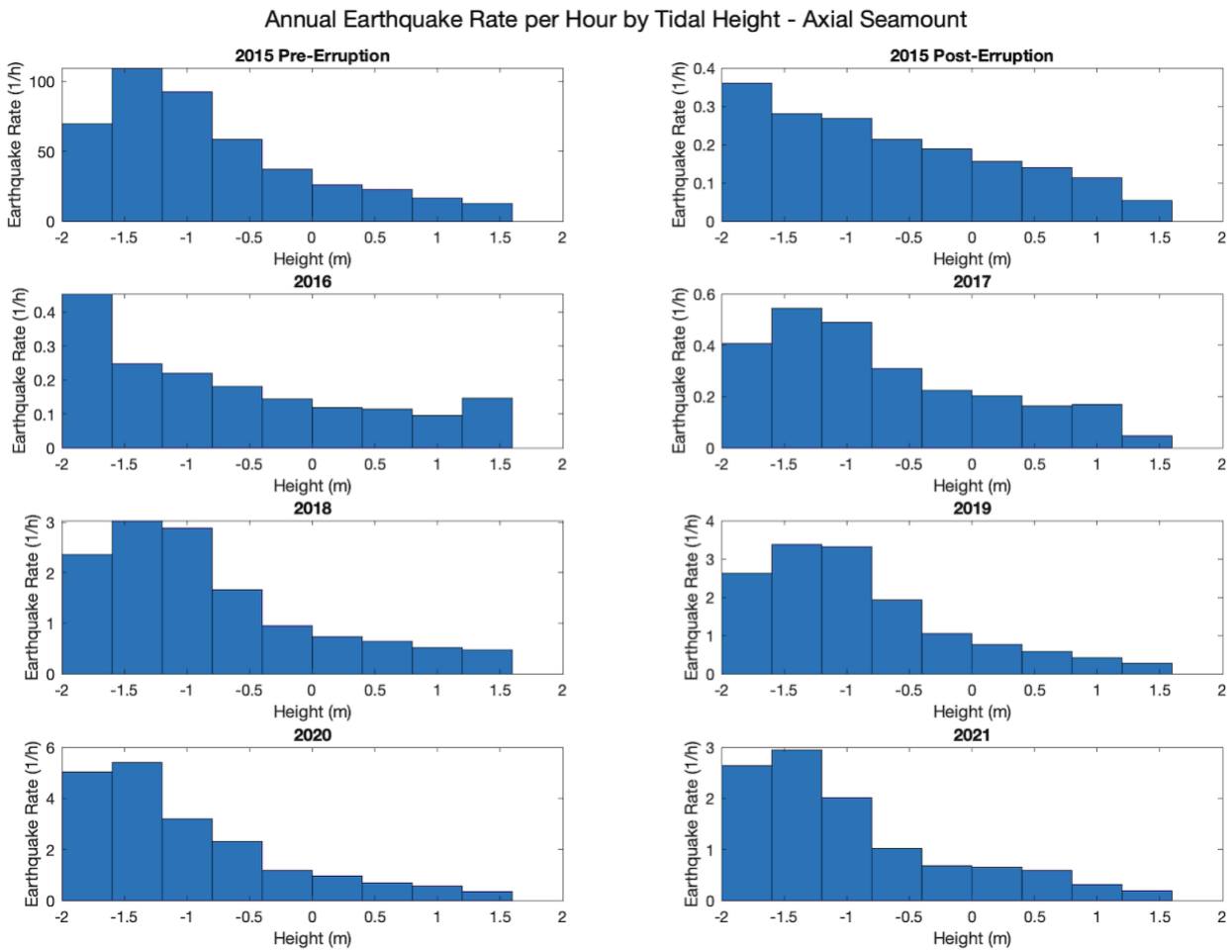

Figure 10. *Panel of annual histograms from June 1, 2015, to December 2, 2021 for post eruption data. January 22, 2015 to April 22, 2015 plots data for 2015 just prior to the eruption, which occurred in 2015. Each histogram plots the rate of earthquakes at different tidal heights per hour on an annual basis. The tidal height ranges from -2m (low tide) to 2m (high tide). The data has been normalized to account for low tide measurements at very low tide heights (~ -1 to -2m) because the primary time that tidal time is spent is near 0m.*

The relative rate of earthquakes from -2m to -1m trends upwards annually (Fig. 11).

Earthquakes at the lowest tides are increasing relative to the average rate of earthquakes among all tidal heights. The slope of this linear trend is 0.24 per year with an R^2 value of 0.95.

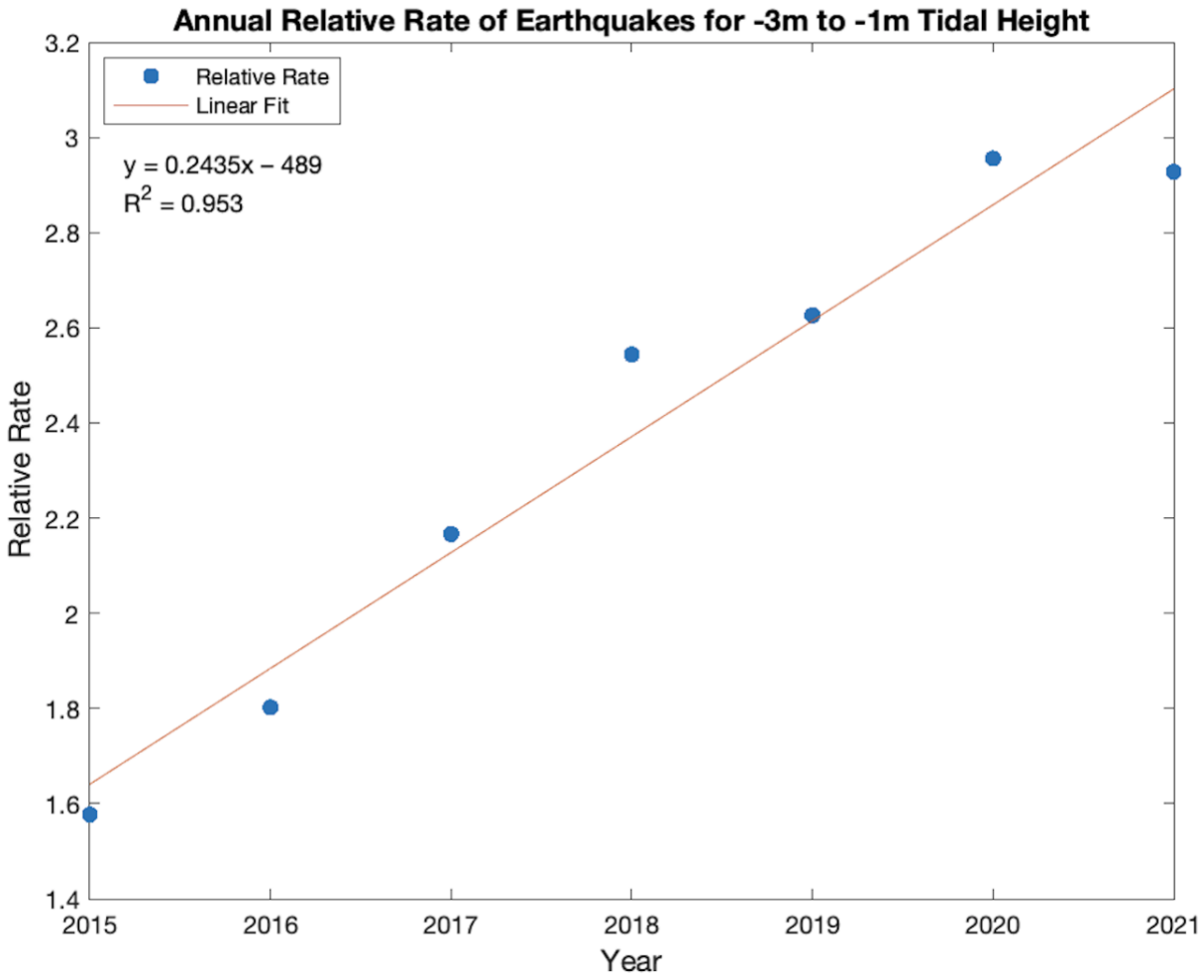

Figure 11. *Scatter plot of the relative rates of earthquakes occurring between -1m and -3m tidal height on an annual basis. The linear fit line was added to the plot, and with a positive slope increasing with time from 2015-2021.*

Data surpassing thresholds of what was seen pre-eruption in 2015 is visible for interpretation in Table 2. The two metrics that have been surpassed are percentage of earthquakes occurring between 150° and 210° and relative rate of earthquakes between -2m and -1m.

Table 2
Annual percentage of earthquakes occurring at tidal phase 150° – 210° and relative rate of earthquakes occurring at tidal height of – 1m to -2m. 2015-Pre represents the measurements just before the last eruption while 2015-Post represents all other data for the 2015 year.

Year	Percentage at Low Tide	Relative Rate at Low Tide
2015 Post-Eruption	23.5	1.6
2016	25.0	1.8
2016	26.5	2.2
2018	31.8	2.5
2019	31.1	2.6
2020	35.8	3.0
2021	32.3	2.9
2015 Pre-Eruption	32.0	2.4

Discussion

Tidal triggering of earthquakes is occurring preferentially during the low tidal phases. For all years, the percentage of earthquakes is far above 17% which is the threshold of total percentage to consider tidal triggering to be a factor. Surpassing a $1/6^{th}$ equal split for the total percentage dismisses the notion that tidal triggering is random. This aligns with the highest rates of earthquakes per hour occurring at the lowest tidal heights. These findings further support the validity of the phenomenon of tidal triggering presented in Tolstoy et al. (2002), and support my hypothesis. Annually, these findings remain consistent with the highest percentage of

earthquakes falling between 150° and 210° presented in Fig. 8. During 2015, 2019 and 2021, the highest percentage of earthquakes strayed out of the 150° to 210° range. The 150° to 210° includes two bins centered on 165° and 195°. During these years, there was a higher percentage in the 225° and 135° bins on the histograms of percentage of earthquakes by tidal phase. However, earthquake percentage was still very high in the 150° – 210° range for those years. At least one of the top two bins by percentage were between this range with the other falling outside of it. The same findings are evident displayed by highest rates of earthquakes at the lowest tidal heights, which supports my hypothesis, and agrees with Scholz et al. (2019).

Annually, the rate per hour is greatest between -2m and -1m tidal heights. Earthquake rate increased substantially as the tidal height decreases below -1m. This means that in proportion to all earthquakes occurring on an annual basis, the change to a lower tidal height during each tidal cycle is triggering earthquakes.

These findings further the idea that the reduction of gravitational stress on the caldera ring fault causes the slip, and earthquakes ensue. As water volume pushing down on the Axial Seamount is reduced during these periods of low tide it causes the slip of the fault, increasing the abundance in earthquakes, (Heaton, 1975). The findings support that tidal triggering is the symptom of increased earthquakes on an annual basis as fraction of earthquakes remains highest at low tidal heights and the low tidal phase.

The positive correlation between year since eruption and earthquake percentage means that tidal triggering is becoming stronger at low tides shown in Fig. 9. The main finding shown by tidal phase and height is that the fraction of earthquakes occurring at low tide are increasing in proportion to the total amount of earthquakes occurring. Tidal triggering of earthquakes increases in strength with time. Although there is a positive correlation, there was a series of

dips in earthquake percentage by tidal phase which occurred between 2018 and 2019, and 2020 and 2021. The dip between 2018 and 2019 decreased less than one percent, but between 2020 and 2021, there was a decrease of 3.5%. This decrease in percentage is due to accounting for percentage of earthquakes between 150° and 210°. During both of these years is when the highest percentage of earthquakes did not occur in both bins between 150° – 210°. Because I only counted the percentage of earthquakes between 150° and 210° for the annual comparison scatter plot, this is an explanation to why there was a decrease between those years. Yet, the positive correlation of the linear trend line certifies the annual increase in the strength of tidal triggering of earthquakes. Both 2020 and 2021 yield an earthquake percentage for 150° -210° that is higher than the percentage which occurred during 2015 just prior to the eruption. The 2020 percentage was 35.8% and 32.3% for 2021. Since the 2015 pre-eruption earthquake percentage at low tidal phase was less than present, data represents the onset of an eruption.

Additionally, the relative rate of earthquakes plotted at the low tidal heights is increasing on an annual basis depicted in Fig. 11. This means that the rate of earthquakes at the low tidal heights are increasing compared to the average rate of earthquakes. The relative rate increases each year except there is a minimal decrease from 2020 to 2021. The relative rate since 2018 – 2021 is higher 2015 pre-eruption numbers. Since the relative rate of earthquakes registers a rate higher than of 2015, we are seeing similar and greater activity to what was seen prior to the last eruption.

Although the relative rate of earthquakes at low tidal height is within the range of pre-eruption numbers, the rate per hour of earthquakes currently is substantially less. Based on previous data from the OOI earthquake catalog, the highest rate of earthquakes per hour is registered just prior to the eruption, shown in Fig. 5. Once the rate of earthquakes per hour

reaches the threshold seen previously is when an eruption will likely be imminent. However, it is important to note that since Axial Seamount is presently inflating much more slowly than it was prior to the 2015 eruption (Chadwick et al., 2021). Therefore, it could erupt sooner without a high rate of earthquakes reflected during 2015. While I cannot predict a specific date that the next eruption will occur, I predict that it will happen soon. This conclusion can be made because eruptions have occurred on a decadal time scale and the previous three eruptions occurred in 1998, 2011 and 2015. The time span between the last two eruptions were approximately 13 years and four years. Just under seven years have passed since the 2015 eruption, giving indication that another eruption is imminent. An explanation to the extended time since that last eruption is that the caldera has not yet reached a new inflation threshold to erupt. The 2015 eruption inflated more than the 2011 eruption, so the next eruption could need to reach a greater threshold which follows the trend presented in Fig. 4. Once the new inflation threshold is met Axial Seamount has the means to erupt.

Conclusion

Findings from this research support my hypothesis that there is a higher fraction of earthquakes occurring at low tide due to the phenomenon of tidal triggering. Tidal triggering of earthquakes is increasing in strength on an annual basis which is depicted in the scatter plots that plot the percentage of earthquakes between 150° and 210° and the relative rate of earthquakes between -2m and -1m. The next steps in further research on this topic would be to track the rate of earthquakes per hour from the OOI catalog to see if rate of earthquakes increases substantially. Additional studies at volcanoes in the ocean and land would be beneficial to determine if there are similar patterns of the seismic data recorded at Axial Seamount. Research

in this sector of marine geology and geophysics is important for understanding seismic activity in the ocean and predicting eruptions at more hazardous volcanoes.

Acknowledgements

I would like to thank Professor William Wilcock for being my mentor and lead help during my research study. Professor Wilcock was instrumental in helping me understand the topic at hand, and providing me the means to be successful in researching the Axial Seamount. I would also like to thank Maochuan Zhang and Zoe Kraus for helping me begin coding my data and understanding MATLAB. The Ocean 445 Teaching Team and students were of great help in helping me write my thesis through tips, peer review and group sessions. Lastly, thanks to those at UW, OSU, NSF, and OOI who funded and made the data available therefore allowing me to carry out this research study.

References

Berg, E. 1966. Triggering of the Alaskan Earthquake of March 28, 1964, and Major Aftershocks by Low Ocean Tide Loads. Nature **210**: 893–896. doi:10.1038/210893a0

Chadwick, J. 2005. Magmatic effects of the Cobb hot spot on the Juan de Fuca Ridge. J. Geophys. Res. **110**: B03101. doi:10.1029/2003JB002767

Egbert, Gary D., and Svetlana Y. Erofeeva. "Efficient inverse modeling of barotropic ocean tides." Journal of Atmospheric and Oceanic Technology 19.2 (2002): 183-204.

Heaton, T. H. 1975. Tidal Triggering of Earthquakes. Geophysical Journal International **43**: 307–326. doi:10.1111/j.1365-246X.1975.tb00637.x

Kelley, D. S., J. R. Delaney, and S. K. Juniper. 2014. Establishing a new era of submarine volcanic observatories: Cabling Axial Seamount and the Endeavour Segment of the Juan de Fuca Ridge. Marine Geology **352**: 426–450. doi:10.1016/j.margeo.2014.03.010

Sahoo, S., B. Senapati, D. Panda, D. K. Tiwari, M. Santosh, and B. Kundu. 2021. Tidal triggering of micro-seismicity associated with caldera dynamics in the Juan de Fuca ridge. Journal of Volcanology and Geothermal Research **417**: 107319. doi:10.1016/j.jvolgeores.2021.107319

Scholz, C. H., Y. J. Tan, and F. Albino. 2019. The mechanism of tidal triggering of earthquakes at mid-ocean ridges. Nat Commun **10**: 2526. doi:10.1038/s41467-019-10605-2

Schuster, A., 1897. On lunar and solar periodicities of earthquakes. Proc. R. Soc. Lond. 61, 455–465. https://doi.org/10.1098/rspl.1897.0060.

Tolstoy, M., F. L. Vernon, J. A. Orcutt, and F. K. Wyatt. 2002. Breathing of the seafloor: Tidal correlations of seismicity at Axial volcano. Geol **30**: 503. doi:10.1130/0091-7613(2002)030<0503:BOTSTC>2.0.CO;2

Vidale, J. E., D. C. Agnew, M. J. S. Johnston, and D. H. Oppenheimer. 1998. Absence of earthquake correlation with Earth tides: An indication of high preseismic fault stress rate. J. Geophys. Res. **103**: 24567–24572. doi:10.1029/98JB00594

Wilcock, W., R. Dziak, M. Tolstoy, and others. 2018. The Recent Volcanic History of Axial Seamount: Geophysical Insights into Past Eruption Dynamics with an Eye Toward Enhanced Observations of Future Eruptions. Oceanog **31**: 114–123. doi:10.5670/oceanog.2018.117

Wilcock, W. S. D. 2001. Tidal triggering of microearthquakes on the Juan de Fuca Ridge. Geophys. Res. Lett. **28**: 3999–4002. doi:10.1029/2001GL013370

Wilcock, W. S. D., M. Tolstoy, F. Waldhauser, C. Garcia, Y. J. Tan, D. R. Bohnenstiehl, J. Caplan-Auerbach, R. P. Dziak, A. Arnulf, & M. E. Mann (2016). Seismic constraints on caldera dynamics from the 2015 Axial Seamount eruption, Science, 354, 1395-1399.

Wilcock, W. S. D., F. Waldhauser, & M. Tolstoy (2017). Catalogs of earthquake recorded on Axial Seamount from January, 2015 through November, 2015 (investigators William Wilcock, Maya Tolstoy, Felix Waldhauser). Interdisciplinary Earth Data Alliance. https://doi.org/10.1594/IEDA/323843.